KfK 4960
November 1991

Coincidence Cross Sections within the Quasi Free Break-up Model for Elastic Projectile Break-up

V. Corcalciuc, H. Jelitto
Institut für Kernphysik

Kernforschungszentrum Karlsruhe

KERNFORSCHUNGSZENTRUM KARLSRUHE

Institut für Kernphysik

KfK 4960

COINCIDENCE CROSS SECTIONS WITHIN THE QUASI FREE BREAK-UP MODEL FOR ELASTIC PROJECTILE BREAK-UP

V. CORCALCIUC and H. JELITTO

Kernforschungszentrum Karlsruhe GmbH, Karlsruhe

Kernforschungszentrum Karlsruhe GmbH
Postfach 3640, 7500 Karlsruhe 1

ISSN 0303-4003

COINCIDENCE CROSS SECTIONS WITHIN THE QUASI FREE BREAK-UP MODEL FOR ELASTIC PROJECTILE BREAK-UP

Abstract

Scrutinizing the basic break-up model of Serber we show that it is possible to derive the triple differential cross sections for particle-particle coincidences in analytical form. An alternative interpretation within the opaque version of the model suggests to assign these cross sections to the elastic nonresonant projectile break-up due to the nuclear interaction. Distortion effects by the Coulomb field of the target are included in analogy to the Serber model. Beside the well known single maximum in the break-up spectra double and triple peak structures appear for certain combinations of the observation angles. The model yields reasonable agreement to the given experimental data, concerning the multiple peak structure as well as the order of magnitude for the absolute normalisation. Its application comprises the region of forward emission angles, especially the angular range of the classical Coulomb deflection.

KOINZIDENZ-WIRKUNGSQUERSCHNITTE IM RAHMEN DES QUASIFREIEN AUFBRUCHMODELLS FÜR ELASTISCHEN PROJEKTIL-AUFBRUCH

Zusammenfassung

Eine eingehende Untersuchung des Aufbruch-Modells von Serber ergab, daß dreifach differentielle Wirkungsquerschnitte für Teilchen-Teilchen-Koinzidenzen in analytischer Form abgeleitet werden können. Eine alternative Interpretation innerhalb des 'opaquen' Modells legt nahe, diese Wirkungsquerschnitte dem elastischen nichtresonanten Projektilaufbruch zuzuordnen, welcher auf der Kernwechselwirkung beruht. Distortionseffekte durch das Coulombfeld des Targets werden mit berücksichtigt in Analogie zum Serbermodell. Neben dem bekannten einzelnen Maximum in den Aufbruchspektren treten bei bestimmten Kombinationen der Beobachtungswinkel Doppel- und Dreifachstrukturen auf. Das Modell befindet sich in vernünftiger Übereinstimmung mit den gegebenen experimentellen Daten, was sowohl die Mehrfach-Peak-Struktur als auch die Größenordnung des Normierungsfaktors betrifft. Die Anwendung umfaßt die Emission in Vorwärtsrichtung und speziell den Winkelbereich der klassischen Coulomb-Ablenkung.

CONTENTS

1.	Introduction	1
2.	Basis for coincidence cross sections	1
3.	Opaque model and elastic nuclear break-up	5
4.	Coulomb corrections	10
5.	Experimental and theoretical data	12
6.	Conclusions	18
Acknowledgement		18
Appendix A.	Calculation of the Jacobian	19
Appendix B.	Remarks on the transparent model	21
Appendix C.	Theoretical cross sections in 3D-plots	22
Appendix D.	Program listing	26
References		29

1. Introduction

The break-up of 190 MeV deuterons was described within a geometrical break-up model, introduced by Serber [1], which served as the basis for several further investigations. Two extreme cases were treated, the *transparent* and the *opaque* model, which describe the idealized cases of a complete transparent and a complete opaque target nucleus. Originally, the model allows to calculate single differential cross sections like energy and angular distributions of the break-up fragments. For the reproduction of the energy spectra of the ejectiles the double differential cross section $d^2\sigma/(d\Omega dE)$ was deduced by Utsunomyia [2] from Serbers formulae. It has been shown that the model reproduces quite well the energy spectra and the angular distributions from the break-up of 156 MeV ^{6}Li-ions at small emission angles [3], measured with the Karlsruhe magnetic spectrograph 'Little John'.

Recently, particle-particle coincidence measurements were performed, where the alpha particle and deuteron fragments were detected in the forward angular range [4 - 7]. The present paper shows that corresponding triple differential cross sections can be derived from the original approach of Serber without any principal modification. Actually, an inaccuracy in the derivation of the expressions within the opaque model has been found and this probably has prevented that the results have been found earlier. Anyhow, the improper intermediate expression in the original article leads again to the correct results and leaves the formulae for the cross sections unchanged.

The Serber model yields good predictions only with a number of certain physical restrictions. The projectile energy should be large compared to the Fermi motion of the projectile clusters and the particle observation should be in forward direction, i.e. in the range of the classical Coulomb deflection angle. With these conditions at least an estimate of coincidence cross sections seems to be possible. As in the article of Serber all results are given in analytical form and can be easily handled.

2. Basis for coincidence cross sections

The projectile (P) consists of two clusters (1) and (2), each with the extension zero and a separation $\mathbf{r}_{12}$, whereas the target nucleus is treated as a circular disc perpendicular to the beam direction with the radius R_T. As already mentioned, the energy of the Fermi motion in the projectile should be small compared to the incident energy.

At the collision one cluster interacts with the target, if it passes the target disc, whereas the other cluster continues undisturbed on its trajectory like a spectator. It follows that the momentum of the observed fragment is the sum of the momentum due to the projectile motion plus the Fermi motion at the moment of collision, which is described by the Fourier

transformed $\tilde{\phi}(\mathbf{p})$ of the relative wave function $\phi(\mathbf{r}_{12})$. Hereby, $\mathbf{p}$ is the relative momentum vector of both clusters. Assuming a Yukawa type wave function

$$\phi(\mathbf{r}_{12}) = \sqrt{\frac{\alpha}{2\pi}} \frac{e^{-\alpha r}}{r}, \quad \alpha = \frac{\sqrt{2\mu\varepsilon}}{\hbar} \tag{2.1}$$

the wave function in $\mathbf{p}$-space is constrained to Lorentzian shape:

$$\tilde{\phi}(\mathbf{p}) = \frac{1}{\pi} \frac{(2\mu\varepsilon)^{\frac{1}{4}}}{(2\mu\varepsilon + p^2)} \tag{2.2}$$

with μ and ε being the reduced mass and the separation energy of both fragments.

In one ideal case the target is assumed to be transparent to the participant fragment which implies that both fragments, after break-up of the projectile, remain quasi undisturbed from the target. The opaque model is based on the assumption of a completely dark target nucleus. It follows that a fragment, once hitting the target disk, undergoes a reaction as ,for example, a complete fusion process and is therefore lost for the detection. Whereas the transparent case is the easier approach the opaque model seems to reflect the physical situation more realistically [3].

We use the coordinate system, introduced by Serber. The x-axis is perpendicular and the y-axis parallel to the target surface. The view upon Fig. 1 is in the direction of the incoming projectiles, which defines the z-direction. For inclusive measurements the opaque model is

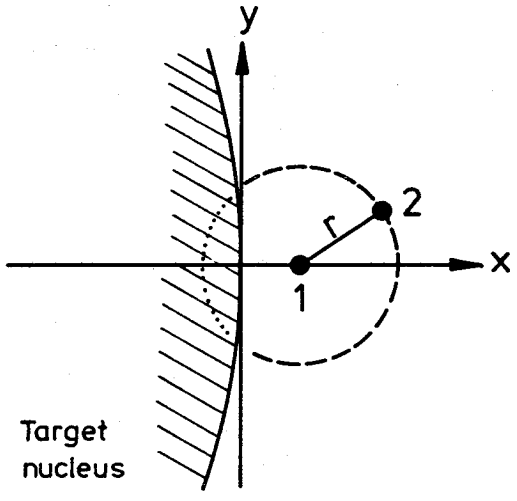

Figure 1. Local coordinate system at the target surface and the two projectile clusters 1 and 2, projected into the x-y-plane with a given separation r. The view upon the figure is in the direction of the incoming projectiles and defines the z-axis, being perpendicular to the x-y-plane.

now characterised by the conditions that the spectator misses and the participant fragment hits the target disc, equivalent to $x_1 > 0$ and $x_2 < 0$. Hereby, as also in the following, the subscribts n and p, used by Serber for the neutron and the proton in the deuteron projectile are replaced by 1 and 2. Taking the Fourier transformed wave function $\tilde{\phi}(\mathbf{p})$ and performing twice a Fourier transformation in the x-coordinate with the above conditions, Serber obtains an expression for the wave function of four independent momentum coordinates

$$\psi(p_y, p_z, p_{x1}, p_{x2}) = \frac{-\hbar^{\frac{1}{2}}}{(2\pi)^{\frac{3}{2}}} \int_{-\infty}^{\infty} \frac{\tilde{\phi}(p_x', p_y, p_z)}{(p_x' - p_{x1})(p_x' + p_{x2})} \, dp_x' \tag{2.3}$$

$$= \frac{-\hbar^{\frac{1}{2}}(2\mu\varepsilon)^{\frac{1}{4}}}{2^{\frac{3}{2}}\pi^{\frac{5}{2}}} \int_{-\infty}^{\infty} \frac{dp_x'}{(p_x'^2 + \mathrm{P}^2)(p_x' - p_{x1})(p_x' + p_{x2})} , \tag{2.3a}$$

$$\mathrm{P} = \sqrt{2\mu\varepsilon + p_y^2 + p_z^2} \, .$$

If the participant fragment hits the opaque target nucleus, it cannot reach the second detector. Therfore, we concentrate on the case that both fragments miss the target nucleus, which is equivalent to $x_1 > 0$ and $x_2 > 0$ in the Fourier transformation. Fig. 1 displays the geometry for a given position of cluster 1 and a given separation r between both clusters. In Serbers approach the part of the circle around cluster 1, overlapping with the target nucleus, is a measure for the probability that cluster 2 hits the target and the projectile breaks up. In our case the part of the circumference outside the target disc yields the probability for the break-up and represents quasi the complementary situation. In other words: Even if both clusters miss the target, an overlap between projectile wave function and target nucleus remains, being the cause for the break-up reaction.

Inspecting the double Fourier transformation, done by Serber, with this new conditions, the resulting wave function ψ in (2.3) remains the same except a minus sign at the beginning. Lateron , only the squared wave function is needed, implying that the condition of 'both fragments missing the target' does not alter the result. This process can be interpreted physically as the elastic nuclear projectile break-up, caused by the fact that the extension of the cluster wave function in **r**-space is deminished by the volume which is superseded by the target nucleus. It has been already described by Glauber [8] and called 'free dissociation' in contrast to the absorptive dissociation.

We now perform the calculation in more detail, which follows the equation (2.3a), since our result deviates from that of Serber. Evaluation of the above integral can be done by performing the contour of integration into the upper half of the complex plane taking into

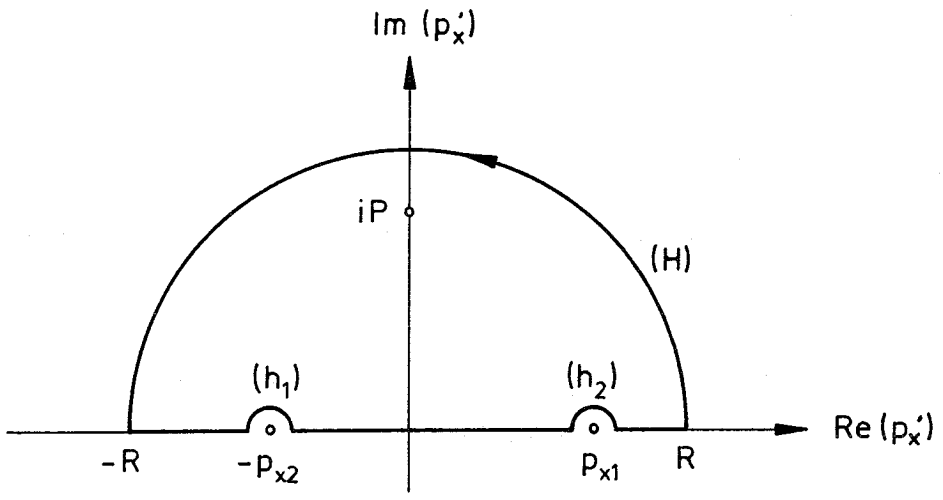

Figure 2. Integration path in the complex plane considering three poles.

account the poles at iP, at p_{x1} and at $-p_{x2}$. Following the path in Fig. 2 and expressing the integrand in (2.3a) by F we get

$$2\pi i\, Res(F, iP) = \int_{-R}^{-p_{x2}-\delta} + \int_{h_1} + \int_{-p_{x2}+\delta}^{p_{x1}-\delta} + \int_{h_2} + \int_{p_{x1}+\delta}^{R} + \int_{H} . \qquad (2.4)$$

Here, δ is the radius of the small half circles around p_{x1} and $-p_{x2}$. After evaluating the integrals we have to perform the limits $R \to \infty$ and $\delta \to 0$. The integral along H vanishes as R goes to infinity. Arranging the terms in (2.4), the integral term in (2.3a), which we name I, then becomes the sum of the residuum at iP and the integrals along h_1 and h_2. These two integrals are easy to calculate [9] and we get

$$I = \frac{\pi}{P\,(iP - p_{x1})\,(iP + p_{x2})} + \frac{i\pi}{(p_{x1} + p_{x2})\,(P^2 + p_{x1}^2)} - \frac{i\pi}{(p_{x1} + p_{x2})\,(P^2 + p_{x2}^2)} . \qquad (2.5)$$

Adding these terms the imaginary part vanishes and we find

$$\psi(p_y, p_z, p_{x1}, p_{x2}) = \frac{\hbar^{\frac{1}{2}}(2\mu\varepsilon)^{\frac{1}{4}}}{(2\pi)^{\frac{3}{2}}} \frac{(P^2 + p_{x1}p_{x2})}{P\,(P^2 + p_{x1}^2)\,(P^2 + p_{x2}^2)} . \qquad (2.6)$$

This wave function differs from the corresponding expression in the article of Serber, represented only by the first term in (2.5). Anyhow, integration of ψ (2.6) over p_{x2}, as the next step in Serbers article, leads to the same result except a normalization factor of 1/2. Lateron (chapter 3) it is shown that for a given detection geometry in most cases two sol-

utions of the given equations, interpreted as near side and far side effect, contribute to the cross section and therefore equalizes the factor 1/2.

The absolute square of ψ (2.6) now represents the differential cross section per unit length of the circumference of the target nucleus, being the quintuple cross section

$$\frac{d^5\sigma_{op}}{dp_y dp_z dp_{x1} dp_{x2} dl} = |\psi(p_y, p_z, p_{x1}, p_{x2})|^2 , \tag{2.7}$$

where l is the length from the x-axis to the break-up point along the circumference of the target nucleus. The subscript 'op' stands for the opaque model. When we omit from now on the indices '1' or '2' for the case that only p_x , p_y or p_z are used, the momenta always refer to the first observed particle.

3. Opaque model and elastic nuclear break-up

The quintuple cross section (2.7) is dependent on the five variables p_{x1}, p_{x2}, p_z, p_y, and l. The desired triple differential cross section $d^3\sigma/(d\Omega_1 d\Omega_2 dE_{1,2})$ in the laboratory system is dependent on the five coordinates θ_1, θ_2, E_1, ϕ_1, and ϕ_2. In order to get directly the laboratory cross section we evaluate the Jacobian

$$\mathbf{J}_{op} = \frac{\partial(p_{x1}, p_{x2}, p_z, p_y, l)}{\partial(\theta_1, \theta_2, E_1, \phi_1, \phi_2)} , \tag{3.1}$$

where θ_1 and θ_2 are the laboratory angles, measured with respect to the beam direction, ϕ_1 , ϕ_2 are the azimuth emission angles of the first and second fragment and E_1 is the laboratory energy of the first fragment.

From Fig. 3 we derive the equations, connecting both sets of coordinates in (3.1) :

$$p_{x1} = p_{\perp 1} \cos\left(\frac{l}{R_T} - \phi_1\right), \tag{3.2}$$

$$p_{x2} = p_{\perp 2} \cos\left(\frac{l}{R_T} - \phi_2\right), \tag{3.3}$$

$$p_{y1} = p_{\perp 1} \sin\left(\frac{l}{R_T} - \phi_1\right), \tag{3.4}$$

$$p_{y2} = - p_{y1} , \tag{3.5}$$

$$p_{z1} = p_{l1} \cos\theta_1 - p_{01} , \tag{3.6}$$

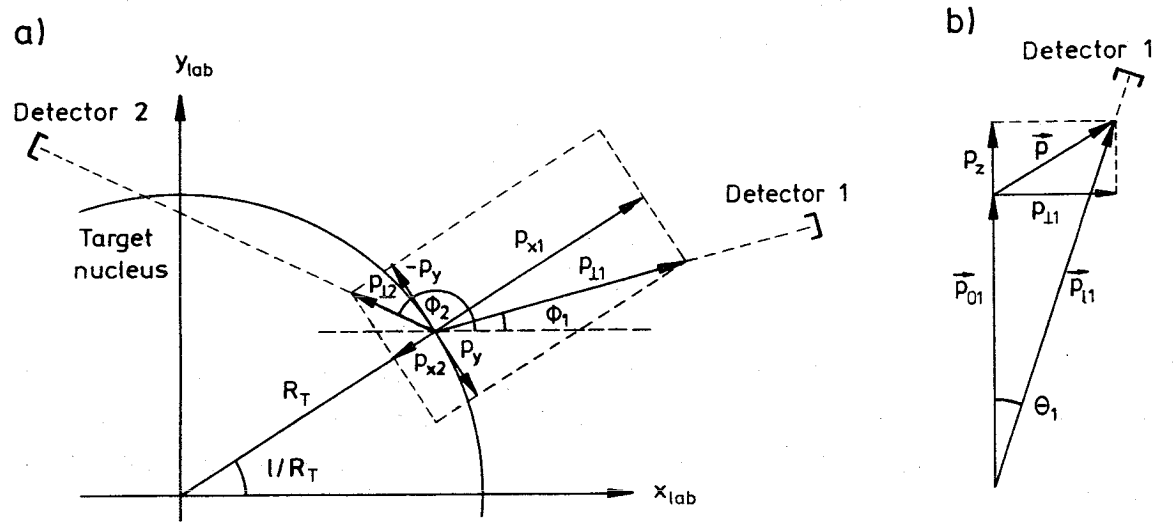

Figure 3. Momenta of the break-up fragments a) in the p_x -p_y plane and b) in the p_z -$p_{\perp 1}$ plane.

and additionally

$$p_{y2} = p_{\perp 2} \sin\left(\frac{l}{R_T} - \phi_2\right), \tag{3.7}$$

$$p_{z2} = p_{t2} \cos\theta_2 - p_{02}\,. \tag{3.8}$$

Hereby, $p_{\perp 1}$ and $p_{\perp 2}$ are the momentum components of the corresponding fragments perpendicular to the beam direction. The momentum p_{01} in (3.6) of the first fragment due to the centre of mass motion of the projectile is $p_{01} = (m_1/m_P)\sqrt{2m_P(E_P - Q)}$, where m_P , E_P , and Q designate mass and energy of the projectile and the Q-value of the break-up reaction. The momentum p_{02} can be obtained analogously. The momenta $p_{\perp 1}$ and $p_{\perp 2}$ are given by

$$p_{\perp 1} = p_{t1} \sin\theta_1\,, \quad p_{t1} = \sqrt{2m_1E_1} \qquad \text{and} \tag{3.9}$$

$$p_{\perp 2} = p_{t2} \sin\theta_2\,, \quad p_{t2} = \sqrt{2m_2(E_P - E_1 - Q)}\,. \tag{3.10}$$

The law of energy conservation is met by using $E_P - Q = E_1 + E_2$ when replacing the energy of the second fragment E_2 in (3.10). The target nucleus is assumed to be infinitely heavy, implying that no recoil energy is transferred.

The Jacobian $\mathbf{J}_{op}$, which includes reactions *in plane* as well as *off plane*, can now be calculated from (3.2) - (3.6), (3.9), and (3.10) (see Appendix A). We find

$$\mathbf{J}_{op} = R_T\, p_{l1}\, p_{t2}^2\, q^{-1}\, m_1 \sin\theta_1 \sin\theta_2 \cos\theta_2$$

$$\text{with} \qquad q = \sqrt{p_{\perp 1}^2 + p_{\perp 2}^2 + 2p_{\perp 1}p_{\perp 2}\cos(\phi_1 - \phi_2)}\ , \tag{3.11}$$

where q is the absolute value of the sum of the transversal momentum components. It represents approximately the momentum transferred to the target nucleus.

Now we combine the quintuple differential cross section (2.7 and 2.6) with the Jacobian (3.11). For a given set of input parameters, corresponding to near side and far side reactions (see Fig. 4) we obtain two solutions. Without any Coulomb correction it can be shown that both solutions are identical, although some momentum components have changed signs. Therefore, the following expression corresponds only to 'one side'. Taking into account that $d\Omega_1 = \sin\theta_1 d\theta_1 d\phi_1$ and $d\Omega_2 = \sin\theta_2 d\theta_2 d\phi_2$ the particle-particle coincidence cross section becomes

$$\frac{d^3\sigma_{op}\,(one\ s.)}{d\Omega_1 d\Omega_2 dE_1} = \frac{R_P\, R_T\, p_{l1}\, p_{t2}^2\, m_1 \cos\theta_2}{4\pi^3 (2\mu\varepsilon)^2 q} \cdot \frac{(1+\xi^2+\zeta_1\zeta_2)^2}{(1+\xi^2)\,(1+\xi^2+\zeta_1^{\,2})^2\,(1+\xi^2+\zeta_2^{\,2})^2} \tag{3.12}$$

$$\text{with} \qquad \zeta_1 = \frac{p_{x1}}{\sqrt{2\mu\varepsilon}}\ , \quad \zeta_2 = \frac{p_{x2}}{\sqrt{2\mu\varepsilon}}\ , \quad \text{and} \quad \xi = \sqrt{\frac{p_y^2 + p_z^2}{2\mu\varepsilon}}\ . \qquad (3.12a-c)$$

Here, $R_P = \hbar/(2\sqrt{2\mu\varepsilon})$ is the average separation of the clusters in the projectile. The other variables have to be replaced using (3.2) to (3.6). In (3.12) the signs of p_{x1} and p_{x2} have to be taken into account. From geometrical considerations it can be derived that $p_{x1} > 0$, only if $(\phi_1 - \pi/2) < l/R_T < (\phi_1 + \pi/2)$ and that $p_{x2} > 0$, only if $(\phi_2 - \pi/2) < l/R_T < (\phi_2 + \pi/2)$.

The 'far side' solution corresponds to the replacements (see Fig. 4) :

$$\begin{aligned} p_{x1} &\rightarrow -p_{x1} \\ \text{and} \quad p_{x2} &\rightarrow -p_{x2}\ . \end{aligned} \tag{3.13}$$

By adding the two contributions the final cross section becomes

$$\frac{d^3\sigma_{op}}{d\Omega_1 d\Omega_2 dE_1} = \frac{d^3\sigma_{op}\,(near\ side)}{d\Omega_1 d\Omega_2 dE_1} + \frac{d^3\sigma_{op}\,(far\ side)}{d\Omega_1 d\Omega_2 dE_1}\ . \tag{3.14}$$

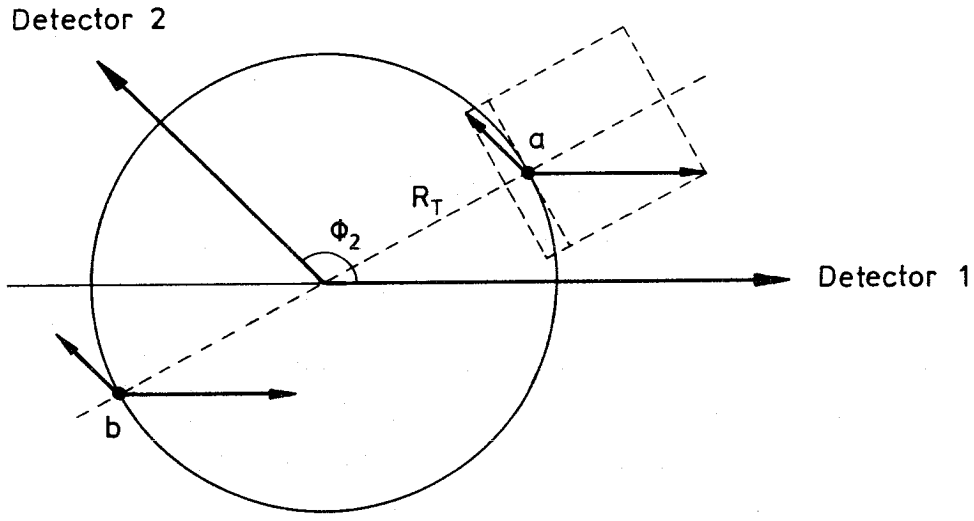

Figure 4. Example of the geometric conditions with the input parameters $\phi_1 = 0°$, $\phi_2 = 135°$ and $p_{\perp 1} = 2p_{\perp 2}$. We obtain $l^{(a)}/R_T = 28.7°$ and $l^{(b)}/R_T = -151.3°$. These angles and the relative lenghts of the vectors at (a) and (b) obey quantitatively to the given set of input parameters. The vectors have the same meaning as in Figure 3a.

When replacing the equations (3.4) and (3.6) by (3.7) and (3.8) the evaluation of the Jacobian shows that it remains the same except that the indices 1 and 2 are interchanged. Physically, it means that at the same detection geometry both fragments are interchanged. So, this complementary situation (first fragment in the second detector and vice versa) can be simply obtained by the interchange of all indices 1 and 2.

The two contributions are added incoherently and since both terms on the right side of (3.14) are identical we simply get a factor 2, which cancels the normalization factor 1/2, mentioned at the end of chapter 2. The situation is completely changed, when including the Coulomb deflection (chapter 4). Some examples of theoretical energy spectra (Fig. 5) show that a single maximum as well double peak and triple peak structures appear. This is caused neither by structures in the projectile wave function, because a Lorentzian shape is used, nor by interference effects, because they are not included in the model. In our approach the structure is due to geometrical and kinematical effects.

In Fig. 5 c) a pole shows up at lower energies. The reason is, that for *in plane* geometry with $\phi_2 - \phi_1 = \pi$, and for a certain fragment energy the momentum transferred to the target nucleus, represented by q in the denominator of the cross section (3.12), becomes zero. In this case the break-up can happen at any place around the target circumference. The position of the pole varies and can be either far away or near to beam velocity energies,

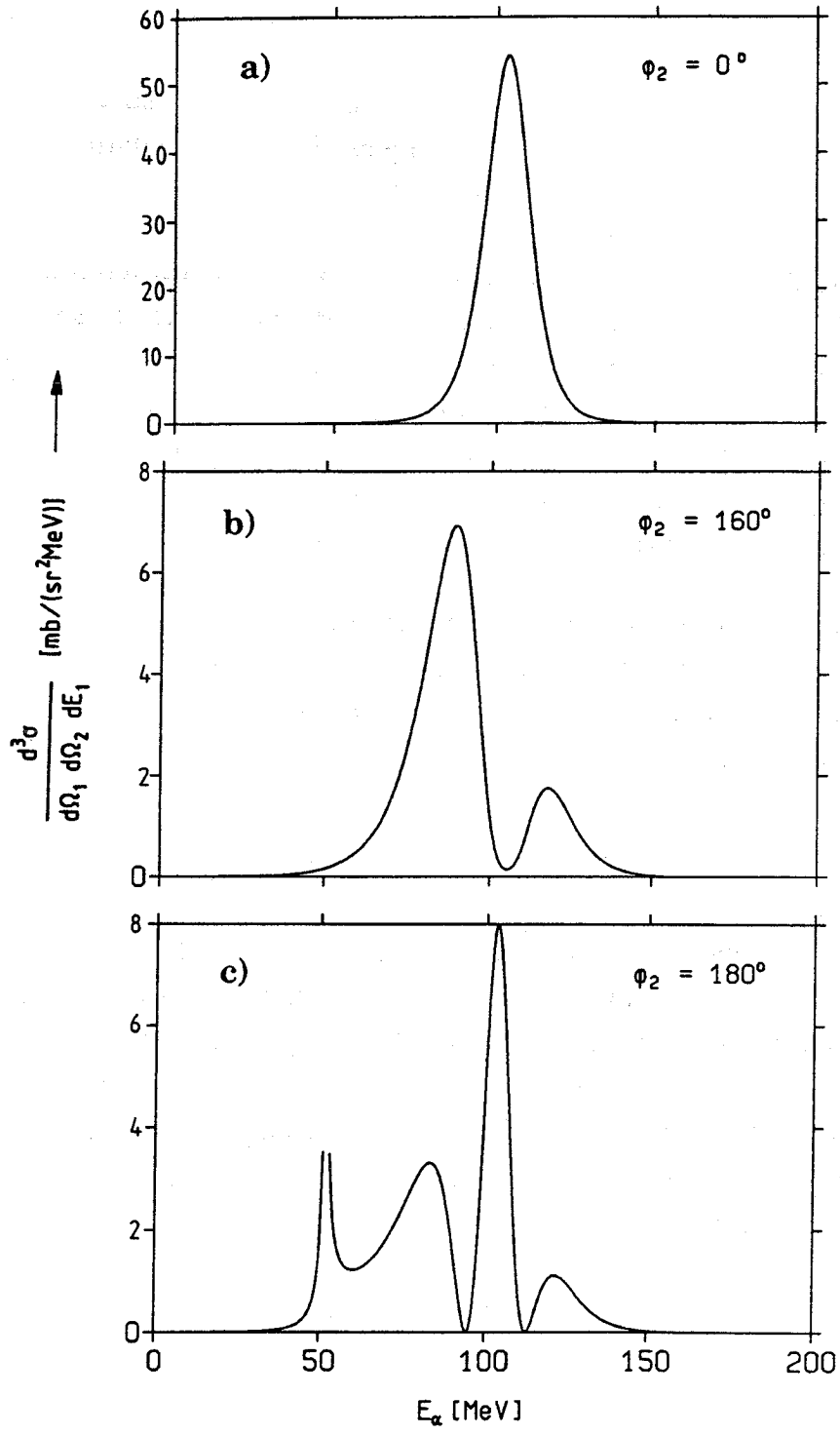

Figure 5. Theoretical coincidence energy spectra of alpha particles for the elastic nuclear break-up, calculated with (3.12) and (3.14) neglecting Coulomb effects. The angles are $\theta_1 = \theta_2 = 6°$ and $\phi_1 = 0°$. The input parameters are taken for the reaction 156 MeV $^6Li + {}^{12}C \rightarrow \alpha + d + {}^{12}C$.

dependent on the observation geometry. Taking into account - more realistically - the 3-body kinematics and also the fact that the target edge is diffuse, it seems reasonable that the increase of the cross section around the pole is smeared out to another maximum.

In order to avoid the pole in the coincidence spectra one could, for example, replace q by $(q + q_0)$, where q_0 is a reasonably chosen small correction. Of course, this could change the cross sections dramatically, if the pole is near to the beam velocity energy. So, we prefer another way. Although we have *in plane*-geometry, given by $\phi_1 - \phi_2 = \pi$, the real reactions do not occur exactly in one plane due to the finite horizontal and vertical acceptances of the detectors and due to the finite size of the beam spot. Geometrical considerations imply that a rough average value for $|\phi_2 - \phi_1|$ is not π, but a little less, because only the absolute value of it is important for the formulae (see A.3 and 3.12c). For comparison with the experimental data in chapter 5 we use $|\phi_2 - \phi_1| = 177°$ instead of $180°$. This is closer to the experimental geometry, avoids the pole and does not alter the equations.

The absolute value of the angular momentum between projectile and target is roughly given, because the impact parameter is equal to the target radius. Now, also the orientation of the angular momentum can be derived easily, because the detection geometry fixes the place of break-up on the target circumference (for $q \neq 0$).

4. Coulomb corrections

The influence of the repulsive Coulomb field between projectile and target in the entrance channel and between fragments and target in the exit channel is taking into account in accordance with Serbers considerations. The effect of bending the trajectory of projectile and fragments is to add a momentum in the direction of p_{x1} and p_{x2} , respectively. This is reasonable because the displacement of the fragments in p_y-direction due to the Fermi motion is negligible when passing the target nucleus. The coincidence cross section (3.12) is altered by the following replacements

$$\begin{aligned} p_{x1} &\rightarrow p_{x1} - \theta_{c1}\, p_{01} \\ \text{and} \quad p_{x2} &\rightarrow p_{x2} - \theta_{c2}\, p_{02}\,. \end{aligned} \tag{4.1}$$

Hereby, θ_{c1} and θ_{c2} are the effective Coulomb deflection angles, caused by the successive deflection of projectile and fragments. Now, the near side and far side term in (3.14) are not any longer identical (Fig. 6). Different charge-to-mass ratios of projectile and fragments have to be considered. The difference of the longitudinal velocity of projectile and fragment due to the Fermi motion also influences the deflection and is represented by an additional factor p_{01}/p_{Π} . We get

$$\theta_{c1} = \theta_c \left(1 + \frac{m_P Z_1}{m_1 Z_P} \frac{p_{01}}{p_{l1}} \right) K , \tag{4.2}$$

$$\theta_c = \frac{Z_P V_C}{2E_P} \tag{4.2a}$$

with Z_P, Z_1, and V_C being the charge numbers of projectile and first fragment and the energy per unit charge due to the Coulomb wall. The factor K is a kinematical factor accounting for the transformation from the c.m. system of projectile and target nucleus to the laboratory system. For small emission angles θ_1 and θ_2 we find in a good approximation $K = m_T/(m_T + m_P)$, which can be derived by considering the centre of mass motion between projectile and target nucleus (m_T is the target mass). The parameter θ_c is defined like in the article of Serber and represents the Coulomb deflection of the projectile before the break-up. The expression for θ_{c2} is analogous to (4.2) with replacement of all indices 1 by 2.

The change of the transversal momenta, affecting the emission angles, has a corresponding longitudinal effect, shifting and deforming the cross sections in the energy spectra. This effect of changing the absolute values of the velocities when approaching the Coulomb wall is considered by replacing the energies as follows [2]:

$$\begin{aligned} E_P &\rightarrow E_P - Z_P V_C \\ \text{and} \quad E_1 &\rightarrow E_1 - Z_1 V_C . \end{aligned} \tag{4.3}$$

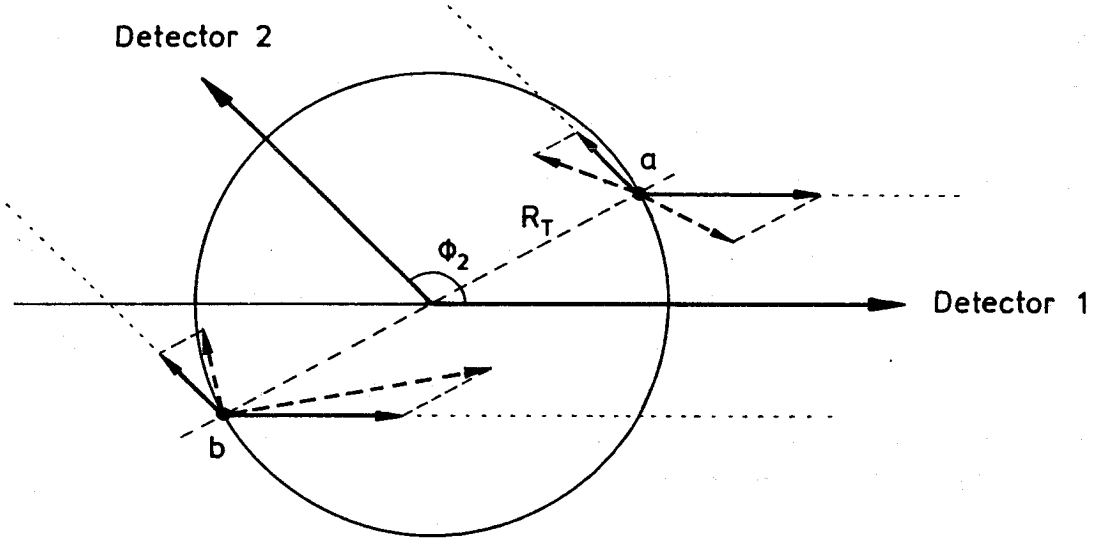

Figure 6. An example with the same geometrical conditions as in Fig. 4 including the classical Coulomb deflection. At near side and far side it has a very different influence on the actual momentum components within the projectile wave function (dashed vectors). The dotted lines show the projected directions to the detectors.

It can be shown that in a good approximation (4.3) is equivalent to

$$p_z \rightarrow p_z - \theta_{cz}\, p_{01} \,. \tag{4.4}$$

In analogy to the Coulomb deflection angle $\theta_{c1} = \Delta p_{\perp 1}/p_{01}$ the parameter θ_{cz} stands for the relative alteration of the longitudinal momentum : $\Delta p_z/p_{01}$. Performing the replacements (4.3) in the expression of p_z (3.6 and 3.9) for small observation angles, one gets θ_{cz} similar to (4.2) :

$$\theta_{cz} = \theta_c \left(-1 + \frac{m_P Z_1}{m_1 Z_P} \frac{p_{01}}{p_{l1}} \right) K, \tag{4.5}$$

with K being added and having the same meaning as in (4.2). For calculation of the Coulomb correction we use the replacements given by the relations (4.1) to (4.3).

5. Experimental and theoretical data

In order to compare the theoretical predictions of the model with the experimental data, the following figures present experimental coincidence cross sections [5,6,7] together with calculated triple differential cross sections given by (3.12) and (3.14). The calculations were performed on a PC using the program compiled in Appendix D.

Fig. 7 gives calculated triple differential cross sections for α and d in the reaction 156 MeV ^{6}Li + T $\rightarrow$ α + d + T, where the target (T) is ^{12}C (Figs. 7 a,b) and ^{208}Pb (Figs. 7 c,d) for V_C = 0 MeV. As expected from (3.12) and (3.14) for both targets in this case the near side (dashed line) is exactly half of the total cross section. Due to the factor R_T in (3.12) the maximum value of the cross sections for the two targets is in the ratio of their radii. As expected, the maximum of the cross section is around beam velocity.

Fig. 8 shows a comparison of theoretical predictions with experimental data for the lead target with θ_1 = 12.68° and variable θ_2, for alpha particle (a,b,c) and deuteron (e,f,g). In the figures the index 1 always refers to the alpha particle and 2 to the deuteron fragment. The theoretical cross sections are multiplied by a normalization factor N = 5. The influence of the vicinity of the pole can still be seen shifting the second bump away from the main one. The position and the width of the maximum is in good agreement with the experimental data. For deuterons the agreement is less satisfactory, especially in the position and magnitude of the second bump. Fig. 9 gives another example for a different observation geometry in the case of lead target for alpha particle ejectiles. The theoretical cross sections are multiplied by a factor N = 10.

In Fig. 10 some results from different detection angles are shown for the case of a carbon target. For alpha particles (a,b,c) the theoretical spectra are multiplied by a factor N = 1/3, whereas for the deuteron fragments (d,e,f) we have N = 1. The experimental spectra have a low statistical accuracy and the broad bump in the alpha particle spectra appears to be shifted by about 10 MeV to lower energies as compared with the theoretical predictions. For

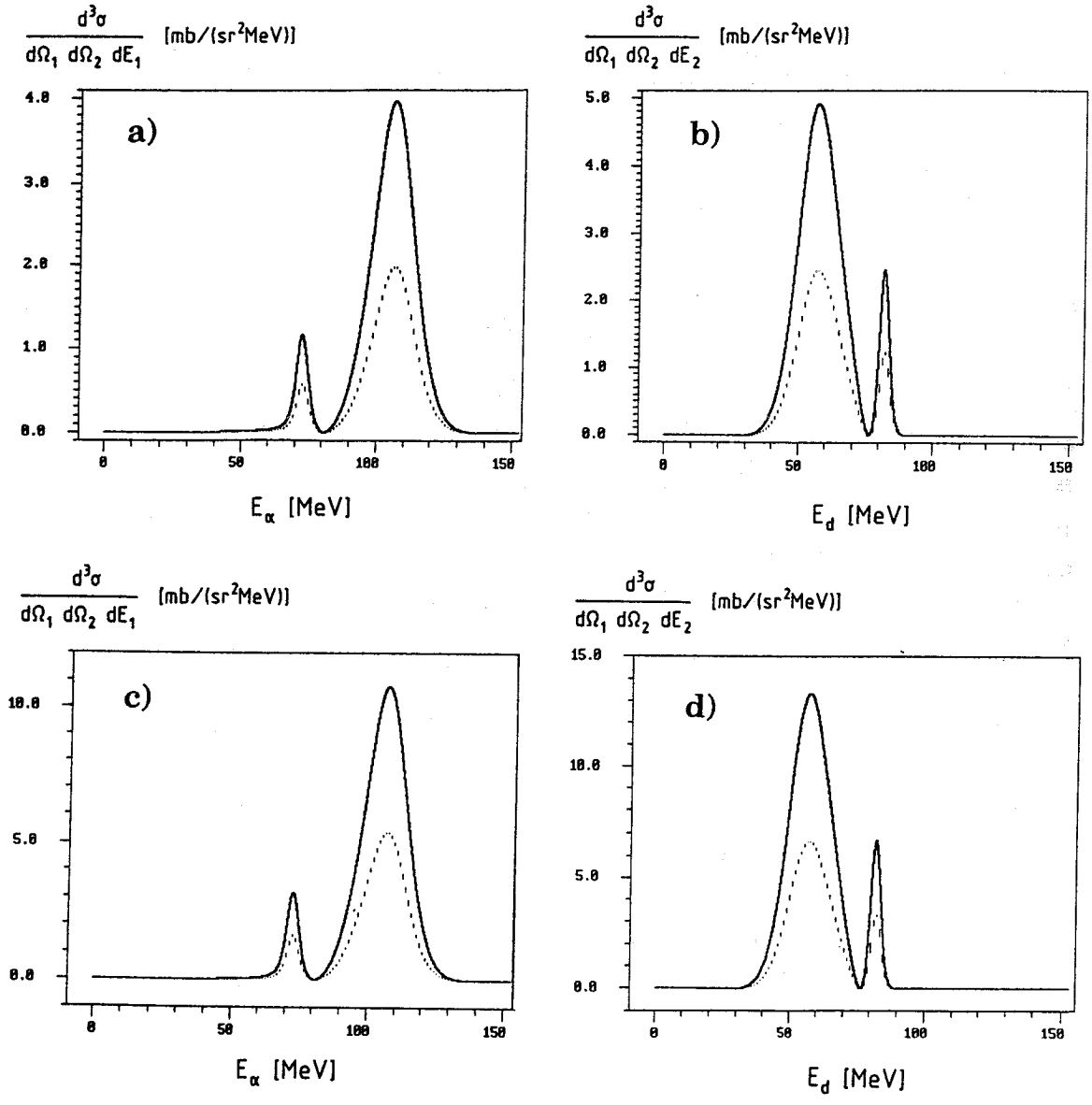

Figure 7. Calculated triple differential cross sections for 156 MeV $^6Li \rightarrow \alpha + d$ break-up in the case $V_C = 0$ MeV , for carbon (a,b) and lead target (c,d). The detection angles are $\theta_1 = 12.68°$, $\theta_2 = 16.88°$, $\phi_1 = 0°$ and $\phi_2 = 177°$. The dashed line represents the contribution from the near side.

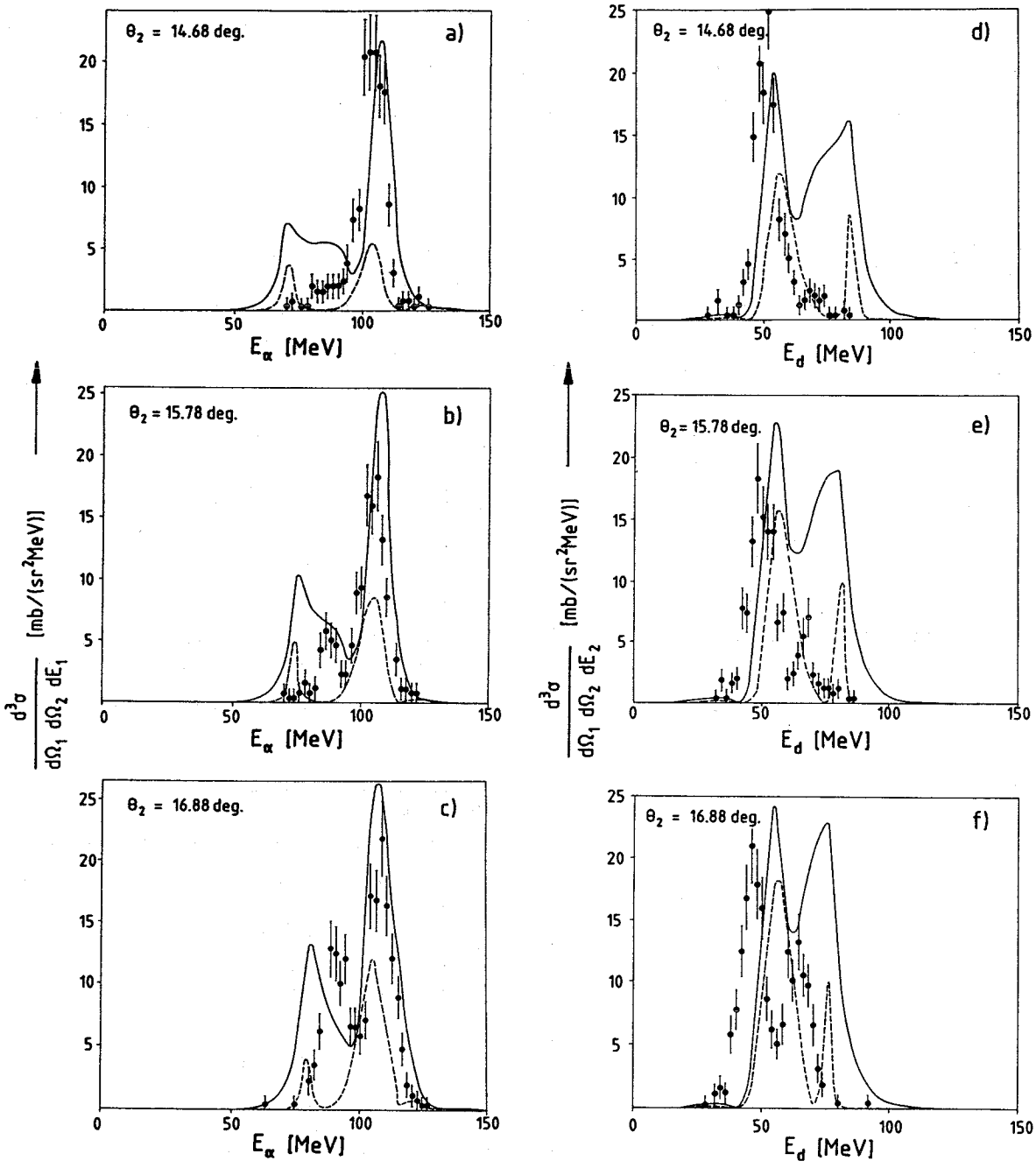

Figure 8. Experimental and calculated triple differential cross sections for 156 MeV $^6Li \rightarrow \alpha + d$ break-up on lead target with the angles $\theta_1 = 12.68°$, θ_2 variable, $\phi_1 = 0°$ and $\phi_2 = 177°$ (180° in the experiment) for alpha (a, b, c) and deuteron ejectiles (d, e, f). The dashed line shows the far side contribution in the alpha spectra and the near side in the deuteron spectra. The theoretical cross sections are multiplied by a factor N = 5.

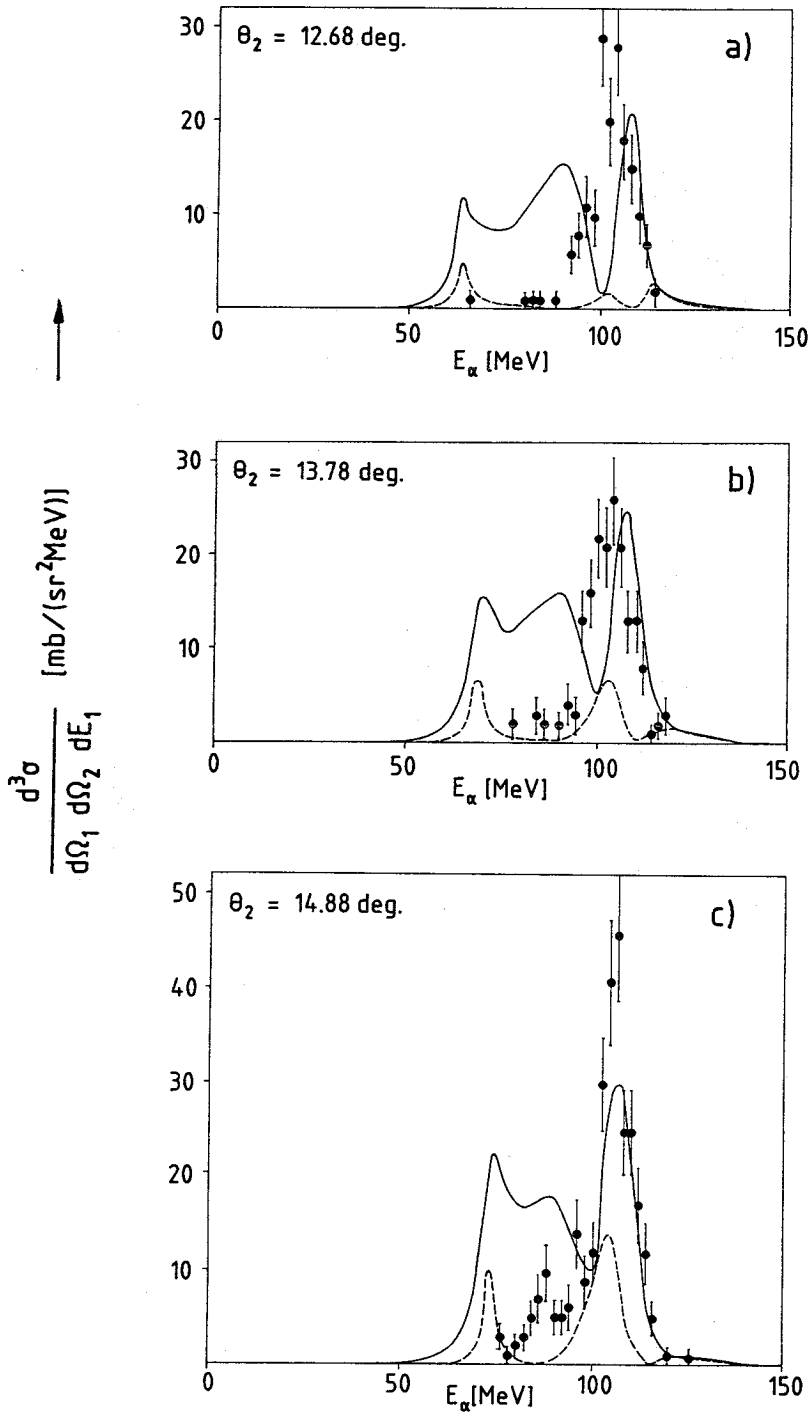

Figure 9. Experimental and calculated triple differential cross sections for 156 MeV $^6Li \rightarrow \alpha + d$ break-up on lead target in the geometry $\theta_1 = 12.18°$, θ_2 variable, $\phi_1 = 177°$ (180° in the experiment) and $\phi_2 = 0°$ for alpha ejectiles. The dashed line shows the far side contribution. The theoretical cross sections are multiplied by a factor N = 10.

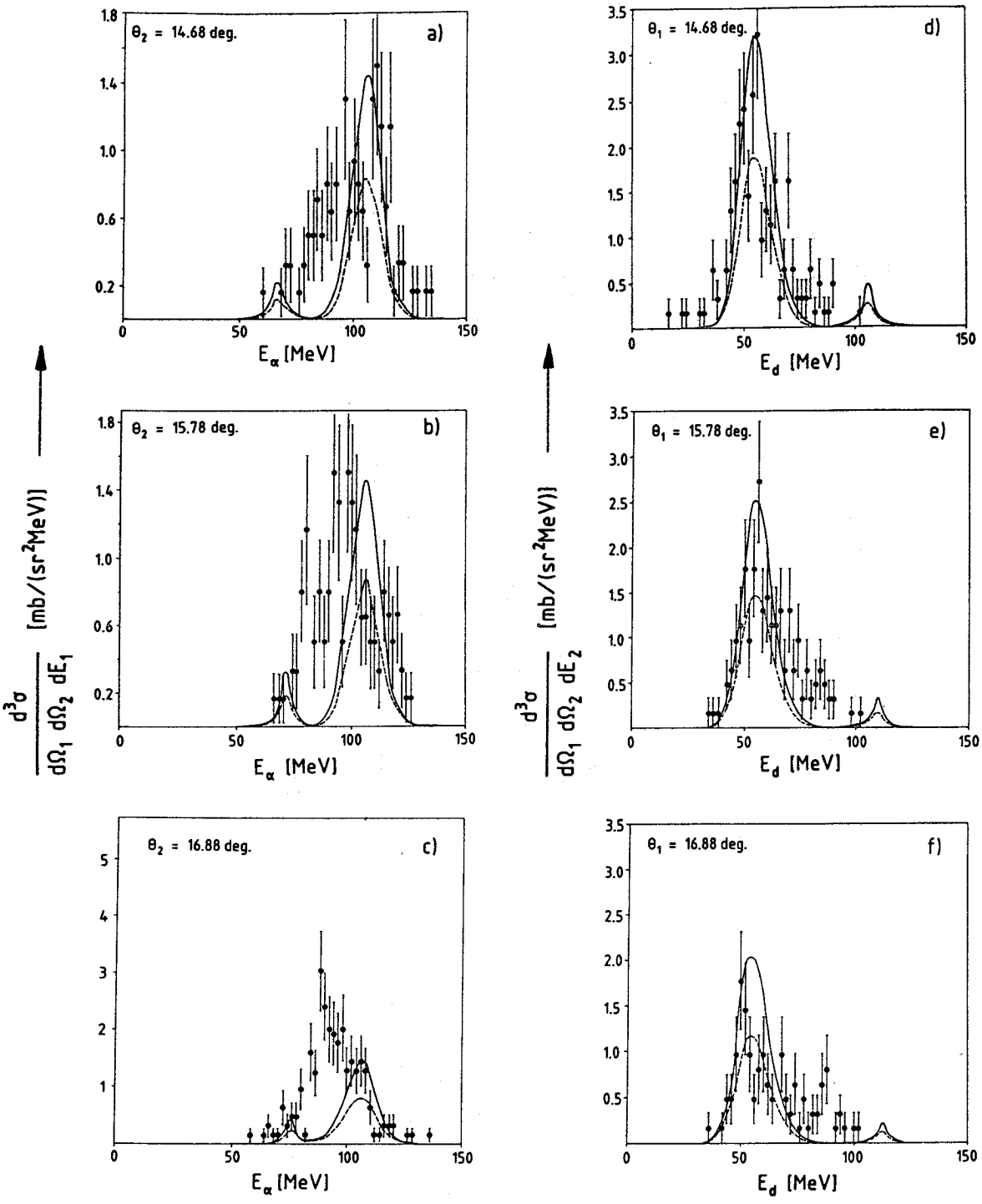

Figure 10. Experimental and calculated triple differential cross sections for 156 MeV $^6Li \rightarrow \alpha + d$ break-up on carbon target with the angles $\theta_1 = 12.68°$, θ_2 variable, $\phi_1 = 0°$ and $\phi_2 = 177°$ for alpha particles (a, b, c). For deuterons we have θ_1 variable, $\theta_2 = 12.68°$, $\phi_1 = 177°$ and $\phi_2 = 0°$ (d, e, f). In the experiment *in plane*-geometry ($\phi_1 - \phi_2 = 180°$) is used. The alpha particle spectra are multiplied by N = 1/3 and for the deuterons the normalization factor is N = 1. The dashed line shows the far side contribution for all spectra.

deuterons the agreement between experiment and theory is rather good. Even the angular dependence on θ_1 is reasonably reproduced. In the experimental data for the carbon target the bumps are broader than for the lead target, probably caused by recoil effects. Note, that the alpha particle spectra and the deuteron spectra belong to different sets of observation angles. In all calculations (Figs. 8 to 11) a value of V_C = 10 MeV is used for the lead, respectively V_C = 5 MeV for the carbon target.

Fig. 11 shows another good agreement between theory and experiment. As before, the theoretical cross sections are multiplied by a factor N = 5. It is mentioned here that the theoretical curves are not adjusted to the measured data, but are fixed by the experimental parameters. The normalisation factor is used for an easier comparison.

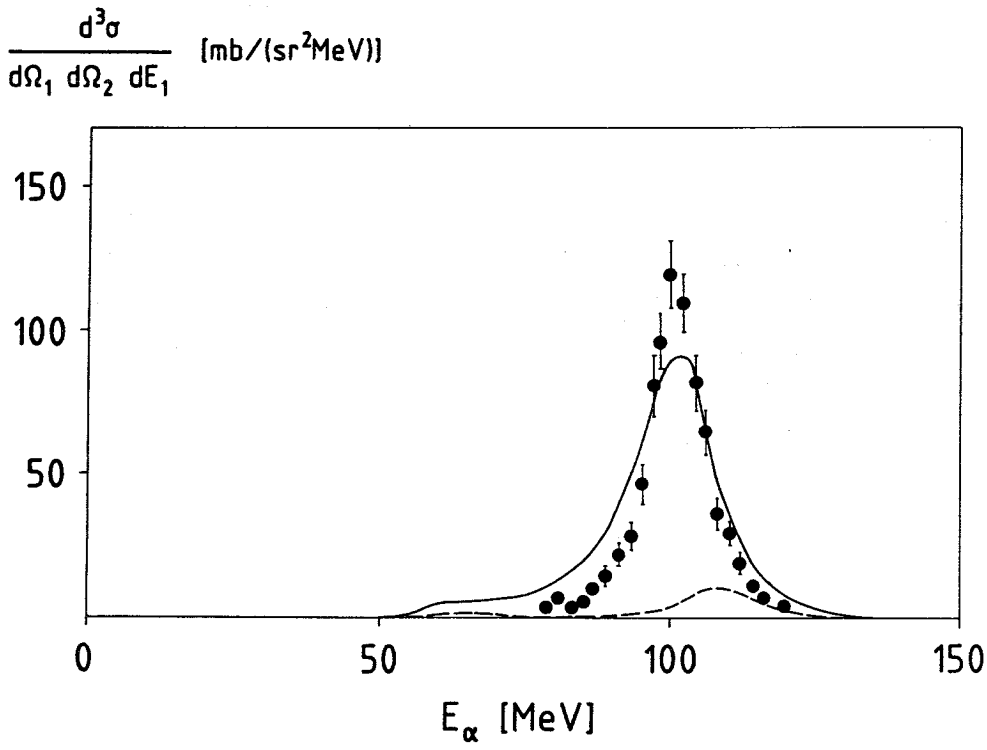

Figure 11. Experimental and calculated triple differential cross sections for 156 MeV $^6Li \rightarrow \alpha + d$ break-up on lead target in the geometry $\theta_1 = 10°$, $\theta_2 = 10°$, $\phi_1 = 0°$ and $\phi_2 = 177°$ (180° in the experiment) for alpha ejectiles. The dashed line shows the far side contribution. The theoretical cross sections are multiplied by a factor N = 5.

6. Conclusions

For the break-up of loosely bound projectiles in the nuclear field of the target nuclei triple differential cross sections for particle-particle coincidences are derived on a simple geometrical model, introduced by Serber, and in the limit of a completely opaque target. A simple and easily applicable analytical formula is obtained, which reproduces the gross features of the experimental data: the order of magnitude of the cross sections, the structures with one or several maxima, the width of the bumps, the dependence of the spectra on geometry, etc.. Nevertheless, the variation of this structure is not as rapid as shown by the observed experimental data.

Taking into account the simplicity of the present approach the results are rather good, showing that many of the important features of experimental triple differential cross sections can be qualitatively explained on simple geometrical and kinematical arguments.

Acknowledgement

We are indebted to Prof. Dr. G. Schatz and to Prof. Dr. H. Rebel for their continuous interest and for their generous support of this studies. We especially thank Math. tech. Assistant H.U. Hohn for providing valuable help in adapting the graphic computer programs (3D-plots) and Dipl. Math. J. Oehlschläger for clarifying several questions concerning the used computer. We are also indebted to Dipl. Phys. J. Wentz for helpful discussions about the model and to Dr. H. Streckwall for useful comments and for verifying the integrations in an alternative mathematical way. We thank Dr. N. Heide for providing the experimental coincidence data and Mrs. E. Frick and Mrs. S. Burkhardt for creating some of the drawings.

Appendix A. Calculation of the Jacobian

The Jacobian for the opaque model (3.1) can be written explicitly as the determinant

$$\mathbf{J}_{op} = \begin{vmatrix} \frac{\partial p_{x1}}{\partial \theta_1} & \frac{\partial p_{x2}}{\partial \theta_1} & \frac{\partial p_z}{\partial \theta_1} & \frac{\partial p_y}{\partial \theta_1} & \frac{\partial l}{\partial \theta_1} \\ \frac{\partial p_{x1}}{\partial \theta_2} & \frac{\partial p_{x2}}{\partial \theta_2} & \frac{\partial p_z}{\partial \theta_2} & \frac{\partial p_y}{\partial \theta_2} & \frac{\partial l}{\partial \theta_2} \\ \frac{\partial p_{x1}}{\partial E_1} & \frac{\partial p_{x2}}{\partial E_1} & \frac{\partial p_z}{\partial E_1} & \frac{\partial p_y}{\partial E_1} & \frac{\partial l}{\partial E_1} \\ \frac{\partial p_{x1}}{\partial \phi_1} & \frac{\partial p_{x2}}{\partial \phi_1} & \frac{\partial p_z}{\partial \phi_1} & \frac{\partial p_y}{\partial \phi_1} & \frac{\partial l}{\partial \phi_1} \\ \frac{\partial p_{x1}}{\partial \phi_2} & \frac{\partial p_{x2}}{\partial \phi_2} & \frac{\partial p_z}{\partial \phi_2} & \frac{\partial p_y}{\partial \phi_2} & \frac{\partial l}{\partial \phi_2} \end{vmatrix} . \qquad (A.1)$$

It is not necessary to calculate all derivatives. One possible way of evaluating the determinant is given here. To simplify the notation we replace the derivatives $\partial p_y/\partial\theta_1$, $\partial p_y/\partial\theta_2$, $\partial p_y/\partial E_1$, $\partial p_y/\partial\phi_1$ and $\partial p_y/\partial\phi_2$ by $p_y^{(1)} \ldots p_y^{(5)}$. With $p_y^{(4)} = -p_y^{(5)}$ (A.1) becomes

$$\mathbf{J}_{op} =$$

$$\begin{vmatrix} \frac{p_{l1}^2 \sin\theta_1 \cos\theta_1 - p_y p_y^{(1)}}{p_{x1}} & \frac{-p_y p_y^{(1)}}{p_{x2}} & -p_{l1}\sin\theta_1 & p_y^{(1)} & \frac{R_T}{p_{x1}}\left(p_y^{(1)} - p_y \cot\theta_1\right) \\ \frac{-p_y p_y^{(2)}}{p_{x1}} & \frac{p_{l2}^2 \sin\theta_2 \cos\theta_2 - p_y p_y^{(2)}}{p_{x2}} & 0 & p_y^{(2)} & \frac{R_T p_y^{(2)}}{p_{x1}} \\ \frac{m_1 \sin^2\theta_1 - p_y p_y^{(3)}}{p_{x1}} & \frac{-m_2 \sin^2\theta_2 - p_y p_y^{(3)}}{p_{x2}} & \frac{m_1}{p_{l1}}\cos\theta_1 & p_y^{(3)} & \frac{R_T}{p_{x1}}\left(p_y^{(3)} - p_y \frac{m_1}{p_{l1}^2}\right) \\ \frac{-p_y p_y^{(4)}}{p_{x1}} & \frac{-p_y p_y^{(4)}}{p_{x2}} & 0 & p_y^{(4)} & R_T\left(1 + \frac{p_y^{(4)}}{p_{x1}}\right) \\ \frac{p_y p_y^{(4)}}{p_{x1}} & \frac{p_y p_y^{(4)}}{p_{x2}} & 0 & -p_y^{(4)} & -\frac{R_T p_y^{(4)}}{p_{x1}} \end{vmatrix}$$

Adding line 4 to line 5, extracting some common factors from the first, second, and fifth row, and adding the fourth row times p_y to row 1 and row 2, the matrix is reduced sucessively to a dimension of 4×4 and then to a size of 3×3. We are left with the expression

$$\mathbf{J}_{op} = \frac{R_T}{p_{x1}p_{x2}} \frac{\partial p_y}{\partial \phi_1} \times \begin{vmatrix} p_{l1}^2 \sin\theta_1 \cos\theta_1 & 0 & -p_{l1} \sin\theta_1 \\ 0 & p_{l2}^2 \sin\theta_2 \cos\theta_2 & 0 \\ m_1 \sin^2\theta_1 & -m_2 \sin^2\theta_2 & \frac{m_1}{p_{l1}} \cos\theta_1 \end{vmatrix} . \qquad (A.2)$$

From equations (3.2), (3.4) and (3.5) one derives the momentum component p_y :

$$p_y^2 = \frac{p_{\perp 1}^2 p_{\perp 2}^2 \, sin^2(\phi_1 - \phi_2)}{p_{\perp 1}^2 + p_{\perp 2}^2 + 2p_{\perp 1}p_{\perp 2} \, cos(\phi_1 - \phi_2)} . \qquad (A.3)$$

After evaluating $\partial p_y / \partial \phi_1$, inserting p_{x1} and p_{x2} and performing further simplifications we get straight forward the final result for the Jacobian $\mathbf{J}_{op}$ (3.11).

Appendix B. Remarks on the transparent model

In case of the transparent version of the Serber model the centre of mass of the projectile will continue its motion undisturbed after the break-up reaction. It follows that the triple differential coincidence cross section is identical to the double differential cross section $d^2\sigma/(d\Omega dE)$ for properly chosen detection angles and is otherwise identical to zero. It means that only the cases 'both fragments hit' or 'both fragments miss the detectors' are possible for the correctly chosen observation geometry.

The situation changes when taking into account the Coulomb deflection. It can be verified that a set of detection angles - also out of plane - fixes the Coulomb deflection angle. This also fixes the impact parameter, which could be much larger than the target radius (Fig. 12). From the physical point of view, here only the Coulomb break-up is a relevant process with rather different characteristics compared to the nuclear break-up. This is not included in the model. Calculations show that coincidence cross sections within this 'transparent' case have characteristics from Rutherford scattering, but not from Coulomb break-up. In principle the calculations could yield informations about the trajectory geometry. Anyhow, this transparent version is not treated further.

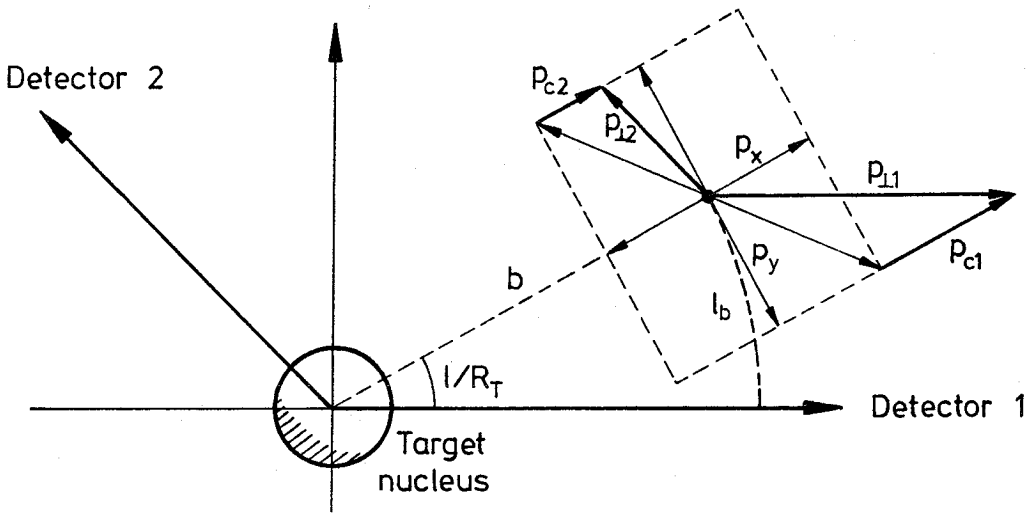

Figure 12. Projection of the momenta into the plane perpendicular to the beam direction for the same set of parameters as in Fig. 4: $\phi_1 = 0°$, $\phi_2 = 135°$ and $p_{\perp 1} = 2p_{\perp 2}$. We get $l/R_T = 28.7°$. If we take $\theta_1 = \theta_2 = 5°$ the deflection angle becomes $\theta_{cb} = 2.46°$, which is classically equivalent to an impact parameter b of 53 fm. To show the proportions a lead nucleus ($R_T = 7.3\,fm$) is drawn schematically. The parameter l_b is the length of the circumference up to the break-up point with the impact parameter b as radius. The parameters l_b and b would replace p_{x2} and l when calculating the Jacobian. Note, that for the transparent case always $p_{y2} = -p_{y1}$ and $p_{x2} = -p_{x1}$.

Appendix C. Theoretical cross section in 3D-plots

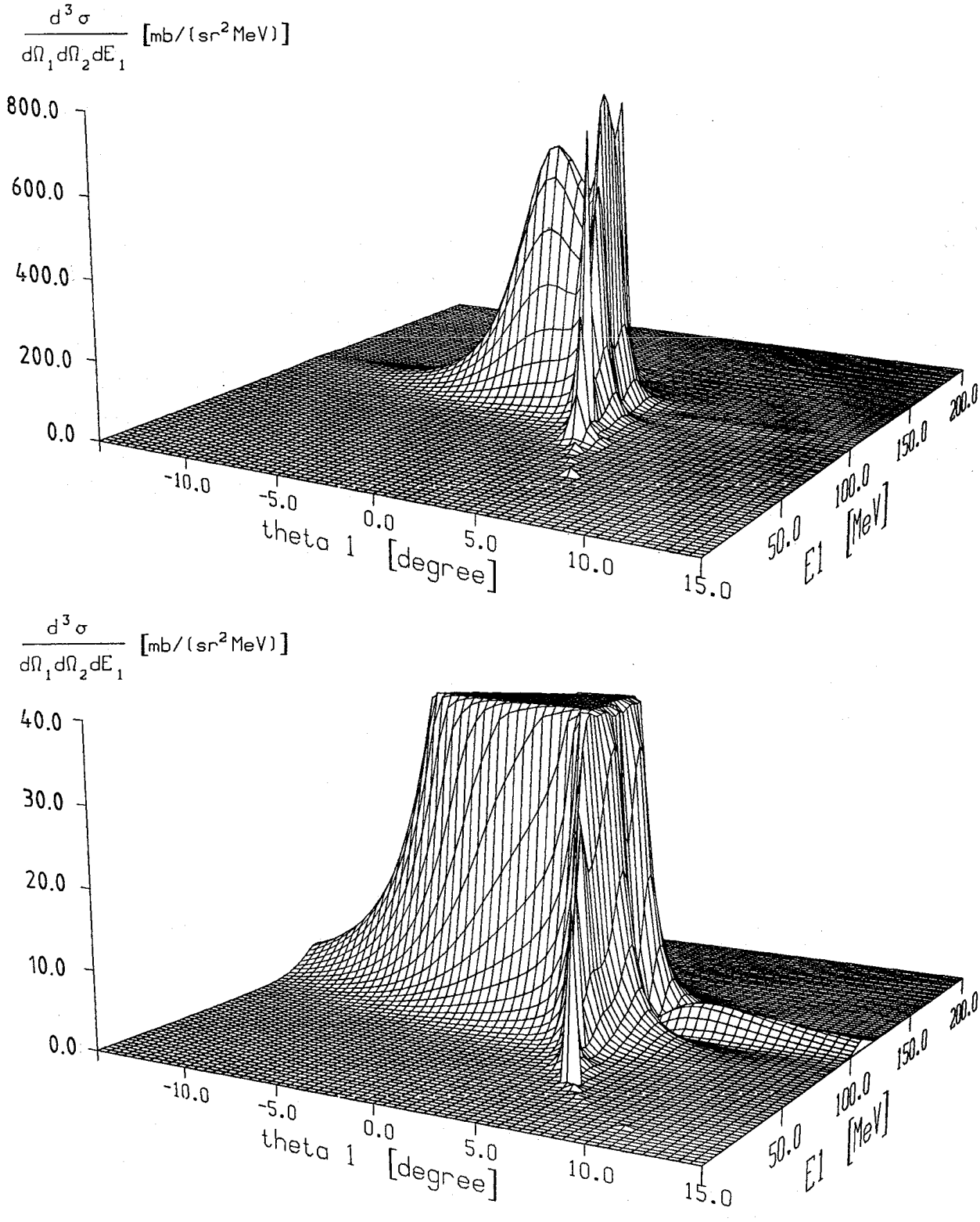

Figure 13. Three-dimensional representation of the triple differential cross section calculated for the elastic nuclear break-up of 156 MeV $^6Li \rightarrow \alpha + d$ as a function of θ_1 and E_1. The alpha particle detection varies from $\theta_1 = -15°$ to $\theta_1 = 15°$, whereas the deuteron detector is fixed at $\theta_2 = -5°$. Coulomb effects are not included ($V_C = 0$ MeV). The same data are shown twice with different vertical scales and are calculated with the program, listed in Appendix D.

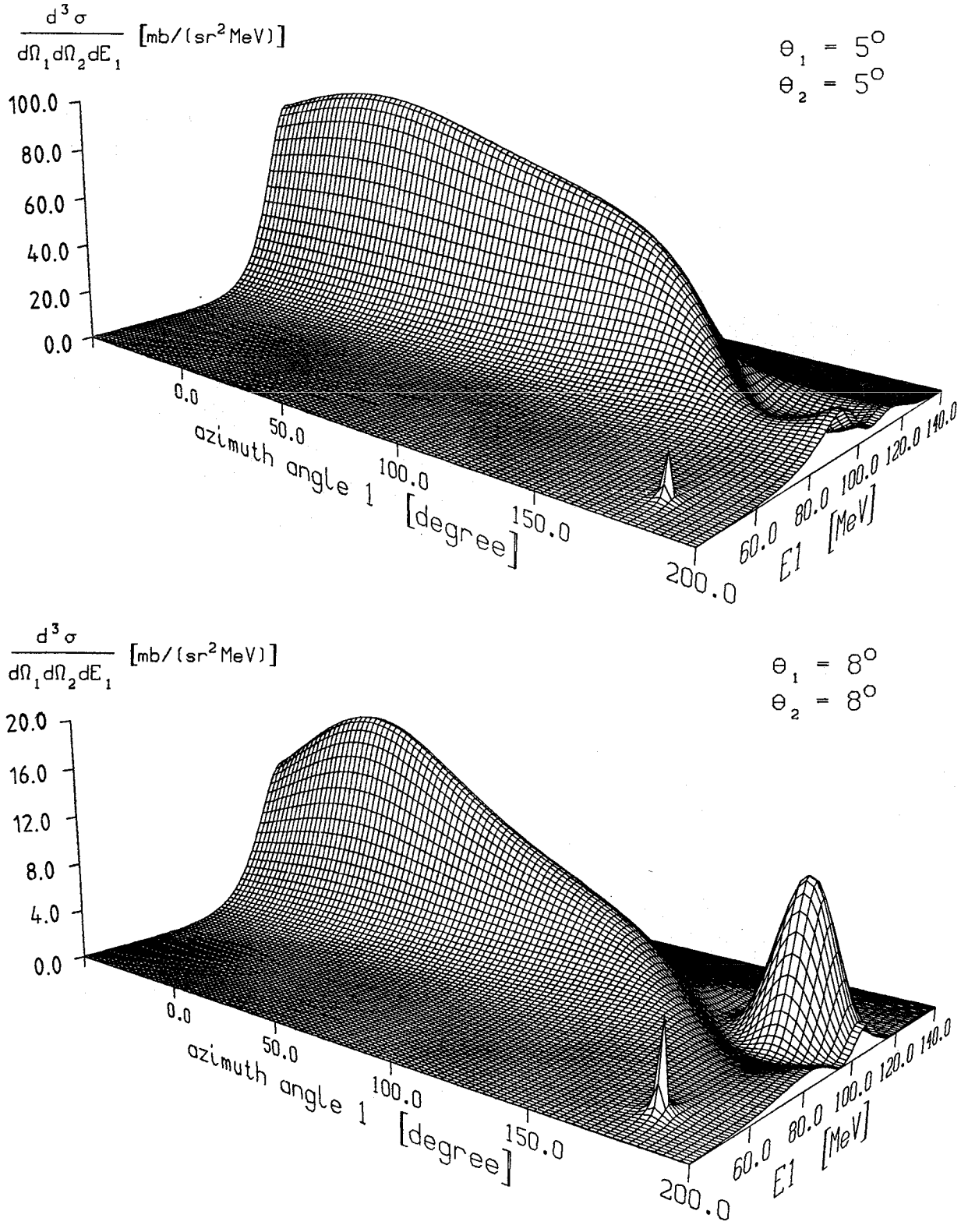

Figure 14. Triple differential cross section for the detection of alpha particles from 156 MeV $^6Li \rightarrow \alpha + d$ as a function of the azimuth angle ϕ_1 and of the alpha particle energy E_1. The azimuth angle of the deuteron detector is $\phi_2 = 0°$ ($V_C = 0$ MeV) . The small peak in the front shows the pole at $q = 0$.

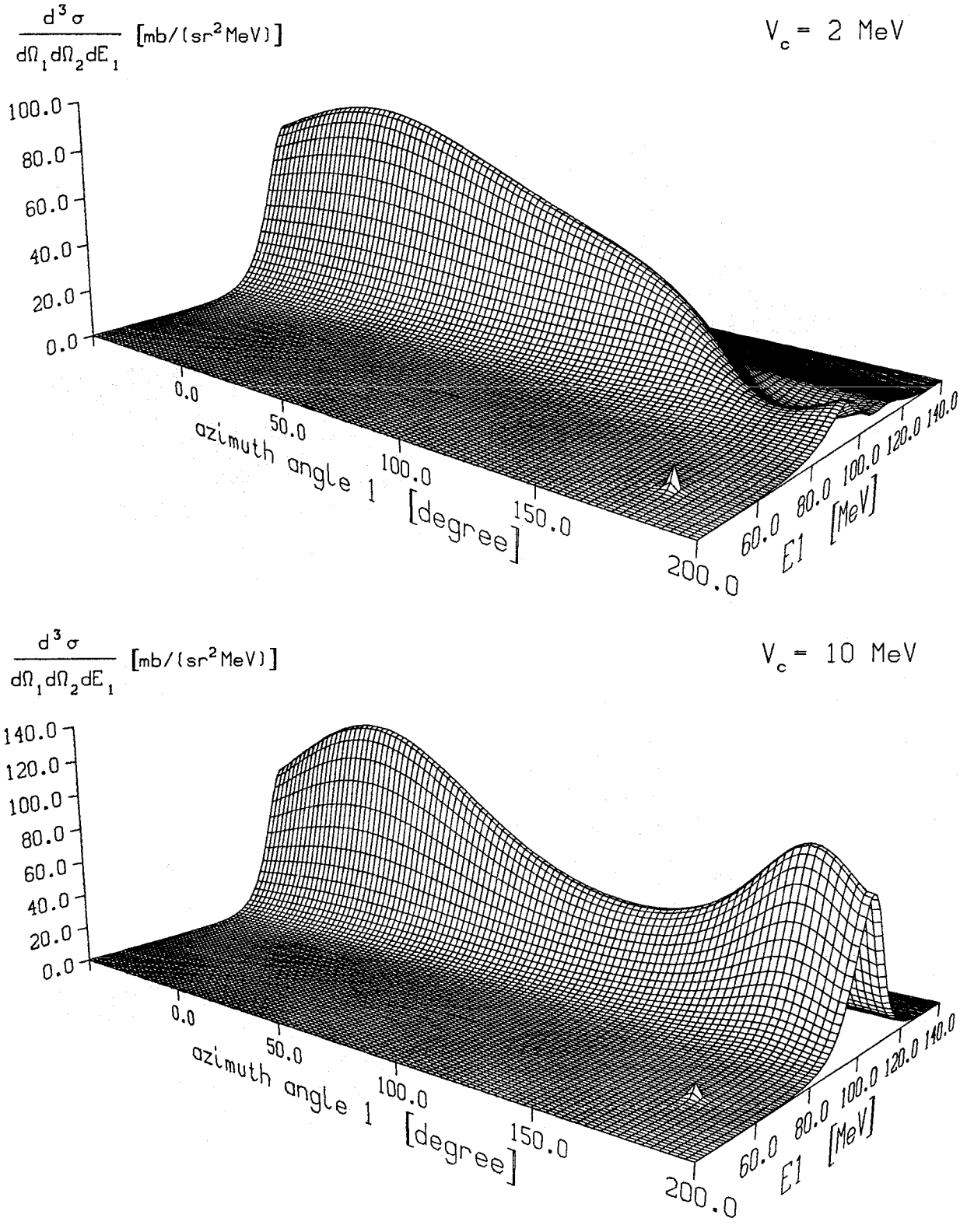

Figure 15. Triple differential cross sections for alpha particles as in Fig. 14 with $\theta_1 = \theta_2 = 5°$. The Coulomb deflection is considered by two different values for the Coulomb wall energy per unit charge. Only the near side contribution is plotted.

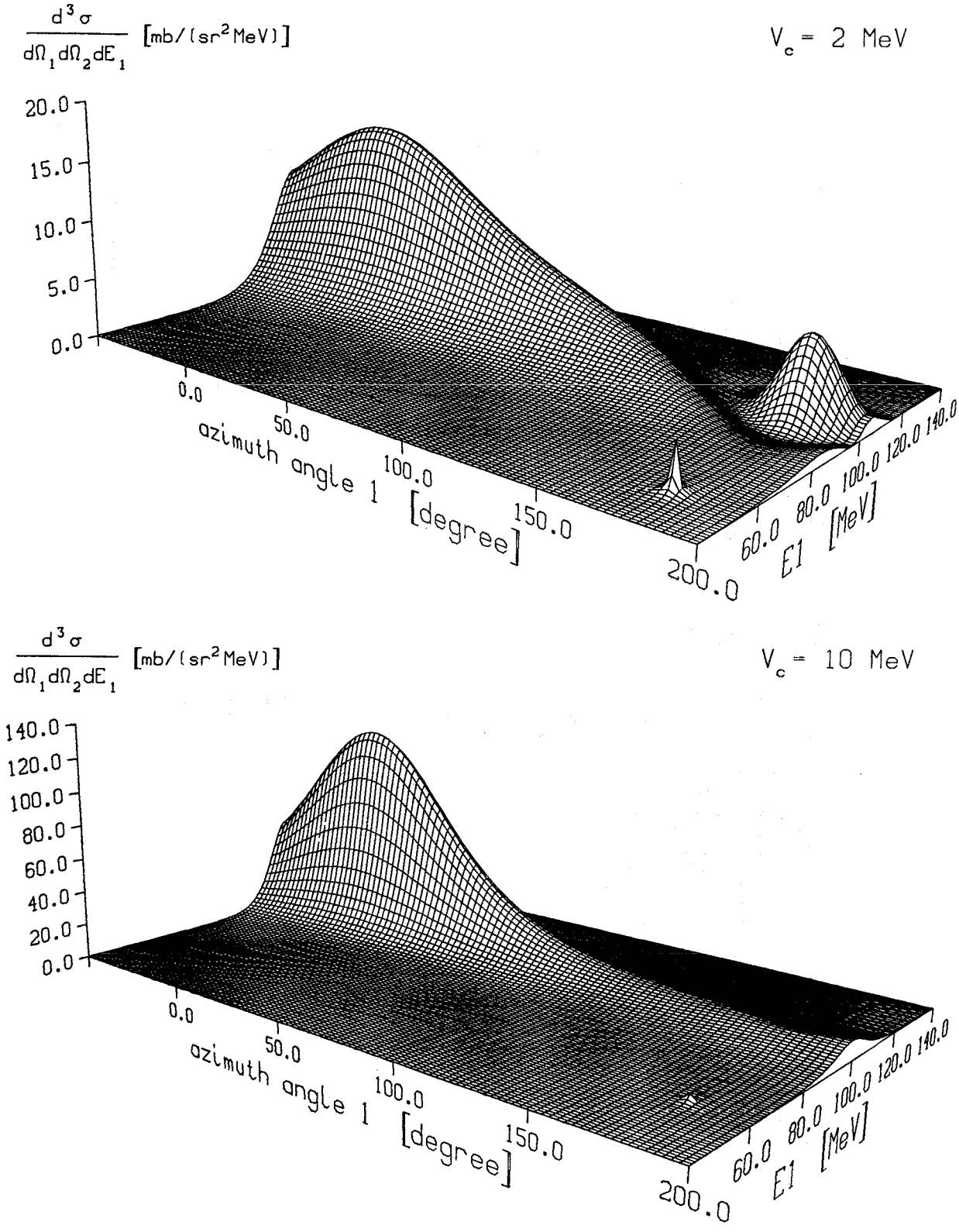

Figure 16. Triple differential cross sections for alpha particles with the Coulomb deflection as in Fig. 15 for the emission angles $\theta_1 = \theta_2 = 8°$, $\phi_2 = 0°$ and for the near side only.

Appendix D. Program listing (FORTRAN 77)

```
      PROGRAM SER

C     *-----------------------------------------------------------------*
C     *                                                                 *
C     *        TRIPLE DIFFERENTIAL CROSS SECTIONS FROM THE              *
C     *        BREAK-UP MODEL OF SERBER (OPAQUE). VERSION 14.10.91      *
C     *        PROJECTILE :  6-Li  -->  4-He + d                        *
C     *        TARGETS    :  12-C  AND  208-Pb                          *
C     *        OPTIONS    :  NEAR SIDE, FAR SIDE, SUM OF BOTH           *
C     *                                                                 *
C     *-----------------------------------------------------------------*

      REAL X(501),Y(501),DY(501)
      IMPLICIT DOUBLE PRECISION (A-H,O-Z)
      CHARACTER CFILEN*32
      COMMON /PARM/AM1,AM2,AMP,AMUE,AKIN,IOUT,ICORR,EPQ,EPC,EMUE,ELAB1,
     & ZP,Z1,Z2,VC,PP,PO1,PO2,QEPS,WJACOF,SIN1,COS1,SIN2,DPHI,SINA,
     & COSA,THETC,PII,PID2,PHIB1,PHIB2,AEXPO,WQNEAR,WQFAR,WQ,WQMAX

C.....PHYSICAL PARAMETERS
      AM1  = 3727.407D0
      AM2  = 1875.627D0
      AMP  = 5601.561D0
      AMUE = AM1*AM2/(AM1+AM2)
      AMTC = 11174.946D0
      AMTP = 193688.563D0
      Z1   = 2.D0
      Z2   = 1.D0
      ZP   = 3.D0
      RP   = 1.63D0
      RTC  = 2.70D0
      RTP  = 7.32D0
      EPO  = 156.D0
      EPQ  = EPO - 1.47D0
C     1.07 MeV DETERMINES THE WIDTH OF THE ALPHA-D-WAVEFUNCTION AND
C     YIELDS THE BEST AGREEMENT TO EXPERIMENTAL INCLUSIVE ENERGY SPECTRA
      EMUE = SQRT(2.D0*1.07D0*AMUE)

C.....INPUT-PARAMETERS
      PII = 3.141592654D0
      PID2 = PII * 0.5D0
      PIGRAD = PII/180.D0
      WRITE(*,'(5X,''OUTPUTFILE                : '')')
      READ(*,'(A32)') CFILEN
      WRITE(*,'(5X,''THETA 1   (DEG)           : '')')
      READ(*,*) THETA1
      THETB1 = THETA1 * PIGRAD
      WRITE(*,'(5X,''THETA 2   (DEG)           : '')')
      READ(*,*) THETA2
      THETB2 = THETA2 * PIGRAD
      WRITE(*,'(5X,''PHI 1     (DEG)           : '')')
      READ(*,*) PHI1
      PHIB1  = PHI1 * PIGRAD
      WRITE(*,'(5X,''PHI 2     (DEG)           : '')')
      READ(*,*) PHI2
      PHIB2  = PHI2 * PIGRAD
      WRITE(*,'(5X,''COULOMB WALL (MeV)        : '')')
      READ(*,*) VC
      WRITE(*,'(5X,''MAXIMUM PLOT-VALUE        : '')')
      READ(*,*) WQMAX
      WRITE(*,'(5X,''12-C (1)  OR  208-Pb (2) : '')')
      READ(*,*) ITARG
      WRITE(*,'(5X,''FRAGMENT  al (1),  d (2) : '')')
      READ(*,*) IFRAG
      WRITE(*,'(5X,''NEAR(1), FAR(2), BOTH(3) : '')')
      READ(*,*) MODE
      WRITE(*,'(5X,''Q-CORR. ?     N(1), Y(2) : '')')
      READ(*,*) ICORR
      WRITE(*,'(5X,''TEST-OUTPUT ? N(1), Y(2) : '')')
      READ(*,*) IOUT
```

```
C.....CHOICE OF THE TARGET
      IF (ITARG.EQ.1) THEN
        AMT = AMTC
        RT  = RTC
      ELSE
        AMT = AMTP
        RT  = RTP
      ENDIF

C.....CHOICE OF THE FRAGMENT
      IF (IFRAG.EQ.2) THEN
        XX  = AM1
        AM1 = AM2
        AM2 = XX
        XX  = Z1
        Z1  = Z2
        Z2  = XX
        XX     = THETB1
        THETB1 = THETB2
        THETB2 = XX
        XX     = PHIB1
        PHIB1 = PHIB2
        PHIB2 = XX
      ENDIF

C.....OTHER CONSTANTS
      EPC = EPQ - ZP*VC
      PP  = SQRT(2.D0*AMP*EPC)
      P01 = PP * AM1/AMP
      P02 = PP * AM2/AMP
      QEPS = 197.33D0/(2.D0*PII*RT)
      THETC  = ZP*VC/(2.D0*EP0)
      SIN1 = SIN(THETB1)
      COS1 = COS(THETB1)
      SIN2 = SIN(THETB2)
      COS2 = COS(THETB2)
      DPHI = ABS(PHIB1 - PHIB2)
      SINA = SIN(DPHI)
      COSA = COS(DPHI)
      PI4 = 4.D0* PII**3

C.....FIXED PART OF THE JACOBIAN AND KINEMATICAL FACTOR
C     THE FAKTOR 10. CONVERTS  fm**2  INTO  mbarn
      WJACOF = RP * RT * 10.D0 * AM1 * COS2/(PI4*EMUE**4)
      AKIN = AMT/(AMP+AMT)

C.....CALCULATION AND SAVING OF THE SPECTRUM
      NPT = 500
      EMIN = 0.D0
      EMAX = 180.D0
      DE = (EMAX - EMIN)/NPT
      DO 10 I=1,NPT+1
        ELAB1 = EMIN + (I-1)*DE
        X(I) = ELAB1
        CALL SERBER
        IF (MODE.EQ.1) Y(I) = WQNEAR
        IF (MODE.EQ.2) Y(I) = WQFAR
        IF (MODE.EQ.3) Y(I) = WQ
        IF (MODE.NE.1.AND.MODE.NE.2.AND.MODE.NE.3) Y(I) = WQ
 10     DY(I)= Y(1)*0.001D0
     THECO1 = THETC * (1.D0+ AMP*Z1/(AM1*ZP)) * AKIN/PIGRAD
     THECO2 = THETC * (1.D0+ AMP*Z2/(AM2*ZP)) * AKIN/PIGRAD
     WRITE(6,*)'  '
     OPEN(UNIT=10,FILE=CFILEN)
     WRITE(10,'(4E15.3)')THETA1,THETA2,PHI1,PHI2
     WRITE(10,'(3E15.3)')VC,THECO1,THECO2
     DO 20 I=1,NPT+1
 20    WRITE(10,*)X(I),Y(I),DY(I)
     CLOSE(10).
     STOP
     END
```

```
C.....TRIPLE DIFFERENTIAL CROSS SECTION IN mbarn/(sr*sr*MeV)
      SUBROUTINE SERBER
      IMPLICIT DOUBLE PRECISION (A-H,O-Z)
      COMMON /PARM/AM1,AM2,AMP,AMUE,AKIN,IOUT,ICORR,EPQ,EPC,EMUE,ELAB1,
     & ZP,Z1,Z2,VC,PP,PO1,PO2,QEPS,WJACOF,SIN1,COS1,SIN2,DPHI,SINA,
     & COSA,THETC,PII,PID2,PHIB1,PHIB2,AEXPO,WQNEAR,WQFAR,WQ,WQMAX
      E1 = ELAB1 - Z1*VC
      E2 = EPC - E1
      ELAB2 = EPQ - ELAB1
      WQNEAR = 0.DO
      WQFAR  = 0.DO
      WQ     = 0.DO
      IF (E1.GT.0.DO.AND.E2.GT.0.DO.AND.
     &  ELAB1.GT.0.DO.AND.ELAB2.GT.0.DO) THEN
        PL1 = SQRT(2.DO*AM1*E1)
        PL2 = SQRT(2.DO*AM2*E2)
        PLAB1 = SQRT(2.DO*AM1*ELAB1)
        PLAB2 = SQRT(2.DO*AM2*ELAB2)
        THETC1 = THETC * (1.DO+ AMP*Z1*PO1/(AM1*ZP*PLAB1)) * AKIN
        THETC2 = THETC * (1.DO+ AMP*Z2*PO2/(AM2*ZP*PLAB2)) * AKIN
        PS1 = PL1 * SIN1
        PS2 = PL2 * SIN2
        Q = SQRT(PS1*PS1 + PS2*PS2 + 2.DO*PS1*PS2*COSA)
        IF (ICORR.EQ.2) Q = Q + QEPS
        IF (Q.NE.0.DO) THEN
          PY  = PS1*PS2*SINA/Q
          PZ  = PL1*COS1 - PO1
          PSQ = 1.DO + (PY*PY + PZ*PZ)/(EMUE*EMUE)
          PX1 = SQRT(PS1*PS1 - PY*PY)
          PX2 = SQRT(PS2*PS2 - PY*PY)

C . . . . DETERMINATION OF THE SIGNS OF PX1 AND PX2
          BL  = 0.DO
          IF (PS1.NE.0.DO) BL = PHIB1 - ASIN(PY/PS1)
          IF (BL.LT.PHIB1-PID2.OR.BL.GT.PHIB1+PID2) PX1 = - PX1
          IF (BL.LT.PHIB2-PID2.OR.BL.GT.PHIB2+PID2) PX2 = - PX2

C . . . . COINCIDENCE CROSS SECTION (OPAQUE MODEL, NEAR-, FAR SIDE)
          ZEN1 = (PX1 - PO1*THETC1)/EMUE
          ZEN2 = (PX2 - PO2*THETC2)/EMUE
          ZEF1 = (- PX1 - PO1*THETC1)/EMUE
          ZEF2 = (- PX2 - PO2*THETC2)/EMUE
          WJACO = WJACOF * PL1 * PL2**2/Q
          WQNEAR = WJACO * (PSQ + ZEN1*ZEN2)**2 /
     &             (PSQ * ((PSQ + ZEN1*ZEN1) * (PSQ + ZEN2*ZEN2))**2)
          WQFAR  = WJACO * (PSQ + ZEF1*ZEF2)**2 /
     &             (PSQ * ((PSQ + ZEF1*ZEF1) * (PSQ + ZEF2*ZEF2))**2)
          WQ = WQNEAR + WQFAR
          IF (WQNEAR.GT.WQMAX) WQNEAR = WQMAX
          IF (WQFAR .GT.WQMAX) WQFAR  = WQMAX
          IF (WQ    .GT.WQMAX) WQ     = WQMAX
        ENDIF

C . . . TEST OUTPUT
        IF (IOUT.EQ.2.AND.ELAB1.GT.100.DO.AND.ELAB1.LT.100.3DO) THEN
          WRITE(6,*)'ELAB1  = ',ELAB1 ,'   PSQ    = ',PSQ
          WRITE(6,*)'PS1    = ',PS1   ,'   PS2    = ',PS2
          WRITE(6,*)'PY     = ',PY    ,'   PZ     = ',PZ
          WRITE(6,*)'PO1    = ',PO1   ,'   PO2    = ',PO2
          WRITE(6,*)'PX1    = ',PX1   ,'   PX2    = ',PX2
          WRITE(6,*)'Q      = ',Q     ,'   THETC  = ',THETC
          WRITE(6,*)'THETC1 = ',THETC1,'   THETC2 = ',THETC2
          WRITE(6,*)'WJACOF = ',WJACOF,'   WJACO  = ',WJACO
          WRITE(6,*)'ZEN1   = ',ZEN1  ,'   ZEN2   = ',ZEN2
          WRITE(6,*)'ZEF1   = ',ZEF1  ,'   ZEF2   = ',ZEF2
          WRITE(6,*)'WQNEAR = ',WQNEAR,'   WQFAR  = ',WQFAR
          WRITE(6,*)'WQ     = ',WQ
          WRITE(6,*)' '
        ENDIF
      ENDIF
      RETURN
      END
```

References

[1] Serber, R.: Phys. Rev. **72** (1947) 1008

[2] Utsunomiya, H.: Phys. Rev. **C30** (1984) 1748

[3] Jelitto, H., Buschmann, J., Corcalciuc, V., Gils, H.J., Heide, N., Kiener, J., Rebel, H., Samanta, C., Zagromski, S.: Z. Phys. **A332** (1989) 317

[4] Kiener, J., Gils, H.J., Rebel, H., Baur, G.: Z. Phys. **A332** (1989) 359

[5] Heide, N.: thesis, Heidelberg (KfK-Report **4551**, 1989)
Heide, N.: KfK internal report, Karlsruhe

[6] Heide, N., Srivastava, D.K., Rebel, H.: Phys. Rev. Lett. **63** No.6 (1989) 601

[7] Heide, N., Rebel, H., Corcalciuc, V., Gils, H.J., Jelitto, H., Kiener, J., Wentz, J., Zagromski, S., Srivastava, D.K.: Nucl. Phys. **A504** (1989) 374

[8] Glauber, R.J.: Phys. Rev. **99** (1955) 1515

[9] Heinhold, J.: "Theorie und Anwendung der Funktionen einer komplexen Veränderlichen", 1. Bd., Leibniz Verlag München (1948) 158